XL CILAMCE
IBERO-LATIN AMERICAN CONGRESS ON COMPUTATIONAL METHODS IN ENGINEERING
NOVEMBER 11-14, 2019
Praiamar Natal Hotel & Convention Natal, RN-BRAZIL

H-TYPE WIND TURBINE PERFORMANCE PREDICTIONS BY A LOW COMPUTATIONAL EFFORT ALGORITHM

Pedro A. A. Baracat[1,2)]
Kamal A. R. Ismail[1)]
pedroaab@gmail.com
kamal@fem.unicamp.br
[1)] *Energy Department, Faculty of Mechanical Engineering, UNICAMP*
Rua Mendeleyev, 200, 13083-860, Campinas/Sao Paulo, Brazil
[2)]*Instituto de Pesquisas Eldorado (Eldorado Research Institute)*
Av. Alan Turing, 275, 13083-898, Campinas/Sao Paulo, Brazil

Abstract. The use of vertical axis wind turbines (VAWTs) has been increasing in recent years. H-type wind turbines may be a good alternative to horizontal axis wind turbines (HAWTs) at places with low space availability, as occurs in cities, low wind velocity and disturbed wind streams, as occurs in areas of mountainous reliefs. Hence, methods of wind turbine performance prediction have become even more important, in wind energy potential studies. They may reduce the number of experimental trials or field tests needed. However, the wind stream behavior on a vertical axis wind turbine is usually complex and hard to predict. A low computational effort algorithm for H-type wind turbine performance prediction was conceived and tested in a regular home computer. At H-type wind turbine simulation, some inputs are the airfoil, air density and dynamic viscosity, chord length or solidity, rotor height and radius, free stream velocity, tip speed ratio range for a constant number of blades (also an input), initial guess and stop criteria of axial induction factor and maximum number of iterations within the stop criteria. For non-Joukowski airfoils, the lift and drag coefficients are given in input tables, changing with the angle of attack and azimuthal angle, from $\pi/180$ (1º) to 2π rad (360º) and step value of $\pi/180$ rad (1º). Each table refers to a specific Reynolds number. The tables are previously analyzed, and missing or non-integer angle values of angles of attack with their coefficients are filled-in by linear interpolation. For Joukowski airfoils, the circle parameters are inputs. The resultant profile and lift coefficients are analytically calculated. The variation of power coefficient with tip speed ratio curves are similar to the literature findings. The predicted power coefficient is 2% higher than the maximum value of experimental results (same tip speed ratio), in a simulation that lasted 34 seconds to run.

Keywords: H-type vertical axis wind turbine, VAWT, Low computational effort, Power coefficient

Nomenclature

R	[m]	Rotor radius
c	[m]	Chord length
a	[-]	Axial induction factor
T	[N]	Thrust over the actuator disk
A	[m²]	Rotor swept are in the actuator disk
H	[m]	Rotor height
N	[-]	Number of blades
L	[N]	lift force
D	[N]	Local instantaneous drag force
Q	[N.m]	Net instant torque
P	[W]	Wind extracted power
V_∞	[m/s]	Free stream velocity
C_l	[-]	Lift coefficient
C_d	[-]	Drag coefficient
R_e	[-]	Local instant Reynolds number
$R_{e,t}$	[-]	Reynolds number for a lift and drag coefficients table
C_T	[-]	Thrust coefficient
V_c	[m/s]	Rotor core velocity
V_w	[m/s]	Downstream velocity
V_r	[m/s]	Relative instantaneous velocity over the airfoil
$R_{e,avg}$	[-]	Reynolds number initial average estimation
C_n	[-]	Local instantaneous normal force coefficient
C_t	[-]	Local instantaneous tangential force coefficient
T_i	[N]	Local instantaneous thrust
C_{Ti}	[-]	Local instantaneous thrust coefficient
Q_i	[N.m]	Local instantaneous torque
F_t	[N]	Local instantaneous tangential force
F_n	[N]	Local instantaneous normal force
C_{Qi}	[-]	Local instantaneous torque coefficient
$\bar{Q}$	[N.m]	Average rotor torque in one revolution
C_Q	[-]	Torque coefficient
P_i	[W]	Local instantaneous wind extracted power
P_{flow}	[W]	Power carried by the flow
C_P	[-]	Power coefficient
a_{i+1}	[-]	New value of axial induction factor
a_i	[-]	Previous value of axial induction factor
λ	[-]	Tip speed ratio
ω	[rad/s]	Rotor angular velocity
θ	[rad]	Azimuthal angle of first blade (reference)
α	[rad]	Local instantaneous angle of attack
ρ	[kg/m³]	Fluid density
μ	[Pa.s]	Fluid dynamic viscosity
σ	[-]	Rotor solidity
θ_i	[rad]	Blade azimuthal angle
$\bar{\lambda}$	[-]	Analysis tip speed ratio average
$\bar{\omega}$	[rad/s]	Rotor angular velocity average
$\lambda_{initial}$	[-]	Tip speed ratio initial value
λ_{final}	[-]	Tip speed ratio final value

Abbreviations

VAWT	Vertical axis wind turbine
D-VAWT	Curved blades Darrieus vertical axis wind turbine
H-VAWT	H-type vertical axis wind turbine
HAWT	Horizontal axis wind turbine
CFD	Computational fluid dynamics
TSR	Tip speed ratio
SST	Single stream tube model
DMST	Double multiple stream tubes model
NACA	National Advisory Committee for Aeronautics

1 Introduction

The first patents on lift-driven vertical axis wind turbines (VAWTs) were introduced in the 1920's, by Georges Darrieus. However, a deeper research started only in the 1970's, on curved blades Darrieus VAWTs (D-VAWTs, Fig. 1a), while the research on H-type vertical axis wind turbines (H-VAWTs, Fig. 1b) became more intense in the 2010's, as described by Möllerström *et al*. [1]. On the other hand, during the same time, the research on horizontal axis wind turbines (HAWTs, Fig. 1c) continued to grow. Therefore, there is a great knowledge gap between HAWTs and VAWTs, which is even greater for the case of H-VAWTs.

The H-VAWT is one variant of Darrieus VAWTs, with straight blades driven by lift forces. In spite of the apparent simple geometry, it is still complex when compared to HAWTs, requiring a reinforced structure to support the mechanical loads. This is one of the reasons for the late development of VAWTs. Due to several prototypes failures, some related to material fatigue, many development programs were cancelled and the reliability on VAWTs has fallen (Möllerström *et al*., [1]). Unsuccessful filed tests may actually highlight the importance of implementing new behavior prediction methods for VAWTs, leading to mechanical analyzes and performance evaluations, instead of discarding their uses. The knowledge gap mentioned is a strong evidence on the unexplored potential for power generation of H-VAWTs.

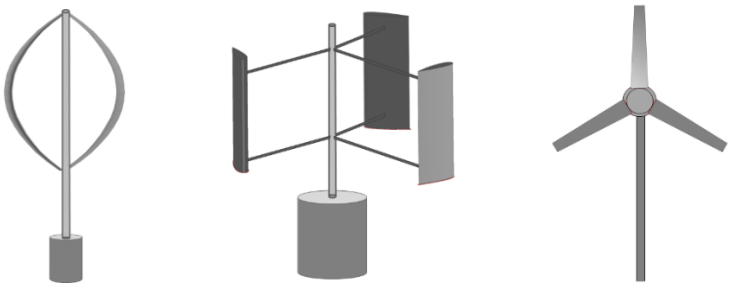

(a) (b) (c)

Figure 1. Wind turbines shapes: (a) D-VAWT; (b) H-VAWT; (c) HAWT

Performance prediction methods on wind turbines have several uses. Each area of implementation has its own characteristics that influence the wind energy generation. Therefore, each implementation case requires particular studies, in order to produce or select ideal rotor geometries and operational parameters for optimization of the aerodynamic efficiency or power coefficient. Those studies include several expensive field tests, due to the high number of variables and their combinations to be evaluated. The prediction of wind turbine behaviors reduce the number of field tests needed, investigating the influence of each design variable and excluding unfeasible cases. Furthermore, they may also lead to simplified and assertive design choices, reducing the time and effort expended in feasibility studies, as well as reducing their costs.

Due to geometrical and physical aspects of VAWTs, their performance prediction methods are more complicated than HAWTs. With complex geometries, VAWTs are composed by structures that disturb the crossing flow, such as the tower and its connections to the blades. The importance of a mechanical balance evaluation is evidenced through this geometry nature. Furthermore, the flow crosses the blades on two occasions, entering at the wind turbine core and leaving it. The first crossing also disturbs the flow, which leads to a complicated physical analysis over its behavior inside the core, as well as in the second crossing through the blades. Furthermore, H-VAWTs are usually not self-starting.

Computational fluid dynamics (CFD) is one of the most popular method of analysis for wind turbines. Depending on the simulation parameters, highly realistic results could be obtained. However, sophisticated CFD simulations on H-VAWTs may lead to high levels of computational effort. Gang and Kau [2] mentioned a computing time from the order of several weeks, in an H-VAWT 3D CFD simulation with unsteady flow. Rezaeiha *et al*. [3] performed high-fidelity CFD simulations for

H-VAWTs on a 24-core super computer, taking approximately 120 hours of computing time each. While CFD methods may fulfill the purpose of reducing the number of field tests needed, they remain expensive for several cases, even with reduced costs compared to field tests. Similarly, CFD analysis may have small impacts on the simplification of design decisions.

The purpose of this work is to present a simple method for the performance prediction of H-type wind turbines, through a validated low computational effort algorithm. The algorithm is based on analytical formulation used to describe H-VAWTs operations. The model is based on the conservation of momentum, actuator disk and enhanced stream tubes. The code was used to perform different simulations for rotors described in the literature and treated by different methods as well as experimental results to establish the validity of the code and predictions, as well as to compare computing times. Parameters such as the power coefficient, wind extracted power, torque, thrust, and computing times were presented and discussed.

2 Methodology

2.1 Overview

In order to produce a low computational effort algorithm, a Matlab code was written. There are two variants of inputs: analysis type and analysis variables. Analysis type inputs are used to define the bases of a simulation, selecting a particular analysis case: Joukowski or regular airfoil, chord or solidity to be used as an analysis variable input (only one needs to be provided, while the other is calculated), direct definition of the flow crossing area or rotor radius definition, initial and constant Reynolds number estimation for the entire analysis or evaluation of Reynolds number at each iteration (using instant values of Reynolds number), interpolation of lift and drag coefficients with the Reynolds number at each iteration or using the closest Reynolds number data on lift and drag coefficients and defining whether graphs with smoothing methods are to be generated with the regular graphs or not. Analysis inputs variables are: name of workspace file, date of simulation, analysis comments, airfoil lift and drag coefficients changing with the angle of attack, in a range of 1º to 360º, for a given Reynolds number, rotor radius, solidity, chord, height, crossing area, fluid density and dynamic viscosity, free stream velocity, number of blades, tip speed ratio values (limits and step value for increment), overall machine efficiency (mechanical, electrical and others), initial guess for the axial induction factor, stop criteria for the axial induction factor, maximum number of convergence attempts on the axial induction factor and the polynomial degree for additional fitting curves generation. It is also possible to set up a second analysis with variable number of blades for a constant (chosen) tip speed ratio.

The tip speed ratio (TSR) is an important parameter, as it may be set as a design variable. It is the ratio between the tip tangential velocity over the free stream velocity. The variation in the values of TSR are related to the angular velocity developed by the wind turbine, which also may be directly set as a design variable instead of TSR. Therefore, curves such as net power, power coefficient, net thrust, thrust coefficient, net torque, torque coefficient and average Reynolds number are often plotted with TSR. The same curves may be also evaluated with the time or the azimuthal angle of a reference blade. In a fixed TSR analysis, time and azimuthal angle are directly related through the rotor's angular velocity, which leads to the same curve shapes. More detailed descriptions are obtained through the evaluation of several outputs with respect of each rotor blade, changing with the time or azimuthal angle as well. In fact, the present method performs calculations for each blade, and the results are showed in overlapping curves, as well as their respective summations. While the net power is a more relevant result than the evaluation of its values at each blade, the local instantaneous torque and thrust are important results for the structure loading and balance. Even the curves that show unsatisfactory balance results are important, as they may suggest the reason of those results, as well as assisting in the elaboration of solutions.

The resulting code is capable to evaluate and predict the most important operating parameters of VAWTs, from the aerodynamic point of view. In a nutshell, those operating parameters are the ones which allow evaluations over the generated power, efficiency, mechanical stresses and manufacturing feasibility.

Since the present work focuses on the aerodynamic evaluation of H-type wind turbines the power coefficient represents the amount of extracted power from the wind stream by the wind turbine. Mechanical and electrical efficiencies are assumed as 0.9. Since the power coefficient depends on the difference between the wind power before and after the rotor, it is adequate method for predicting the variation of several parameters such as the thrust, torque, power curves with TSR, azimuthal angle and time. This represents an advantage of the present method, due to the complex nature of the flow inside the turbine core, which no longer needs to be included in details. However, an overall mathematical description is still necessary.

For the description of the flow inside the H-VAWT core, the axial induction factor is introduced. It defines numerically the change in the flow velocity when crossing rotor (assuming a hypothetical) disk. Since the flow velocity at the core change for each position, also depending on the instant position of the blades, the axial induction factor needs to be converged in a value that leads to a good representation of the overall flow behavior at the core, for each calculation step of this method. As a consequence, instant flow velocities at the core are generated, representing the disturbed streamlines inside it. From the core velocity, the downstream velocity may be estimated, which allows the estimation of an average instant difference in the flow velocity. Direct mathematical relations between the values of axial induction factors and the net thrust, thrust coefficient, torque, torque coefficient, power and power coefficient can be analytically derived.

The power associated to the flow depends on its velocity. With an estimation on the difference of the flow velocities before and after passing through the rotor, the extracted power can be estimated, as well as the power coefficient. From the upstream, core and downstream velocities it is also possible to evaluate the local instantaneous flow velocities over the blades, which are necessary, among other variables, for the local instantaneous Reynolds number estimation and local instantaneous angle of attack calculation. From the obtained values, the equivalent lift and drag coefficients can be selected in the input tables, often filled with experimental values (Sheldahl and Klimas [4]), leading to the local instantaneous lift and drag forces calculations. The local instantaneous thrust and torque are calculated composing those forces. With the angular velocity and the net torque, the net power can be estimated in a different and more realistic way, since experimental data is involved (Sheldahl and Klimas [4]). This is the case for the net thrust and torque calculations as well. As described before, the net thrust and thrust coefficient can be estimated through the axial induction factor. This usually leads to different outcomes in comparison with the thrust and thrust coefficient calculated through the lift and drag coefficients and forces.

For the mechanical stress evaluation, the resulting curves of thrust and torque need to be analyzed. While the thrust describes the loading forces over the blades or other wind turbine structures, the torque is related to the power generation. However, it may also assist in a mechanical stress evaluation, especially for the case of VAWTs. The mechanical stresses over a HAWT are often evaluated from the force loading over the blades and the resultant forces over other structures, such as the tower. In a VAWT, those analyses are also necessary. However, it is also necessary to evaluate the balance of the turbine, which describes the overall fluctuations of thrust and torque over the structure. It is desirable that the summation of the torque and thrust generated by each blade in a VAWT produce smooth and non-fluctuating curves of total torque and thrust with time or azimuthal angle, with the lowest variations between minimum and maximum values.

In order to perform these calculations, a Matlab code based on the momentum conservation model, is applied to actuator disk and stream tube models. As described by Mikkelsen [5], the actuator disk model was introduced by Froude [6], and considers the wind turbine as a solid disk covering the flow crossing area, in which the wind power is extracted. In this work, a single stream tube (SST) based method was implemented in combination to the actuator disk. The SST was proposed by Templin [7] and assumes the flow velocity constant at the rotor's core as a simple assumption. Other methods were derived from the SST, as the case of the double multiple stream tubes model (DMST), that considers several double stream tubes over the rotor (each divided in upwind and downwind), leading to different core velocities.

The present method is conceived with the aim of balancing the simplicity of SST (leading to a low computational effort), and the quality of results produced by the DMST. Instead of dividing the rotor in

more stream tubes, the analysis is performed following the entire revolution of each blade, in steps of azimuthal angle. The assumption of constant core velocity from SST is carried by the method. However, for each interpolation or step, the core velocity changes, converging to an optimum value for each calculation case, as in the case of the axial induction factor.

The first variable to be incremented is the TSR. For each TSR value, the azimuthal angle is also incremented. A third iterative analysis is carried for each blade of the rotor. Inside this last analysis, the induction factor, core velocity and downstream velocity are converged. They are considered constant for the entire VAWT, changing at each convergence calculation and each step of blade being analyzed, azimuthal angle and TSR. Once they are converged, the values are used to calculate local instantaneous values of the flow velocity over the blade, angle of attack and Reynolds number as well as local instantaneous and net values of lift force, drag force, normal force, normal force coefficient, tangential force, tangential force coefficient, thrust, thrust coefficient, torque, torque coefficient, power and power coefficient (Fig. 2).

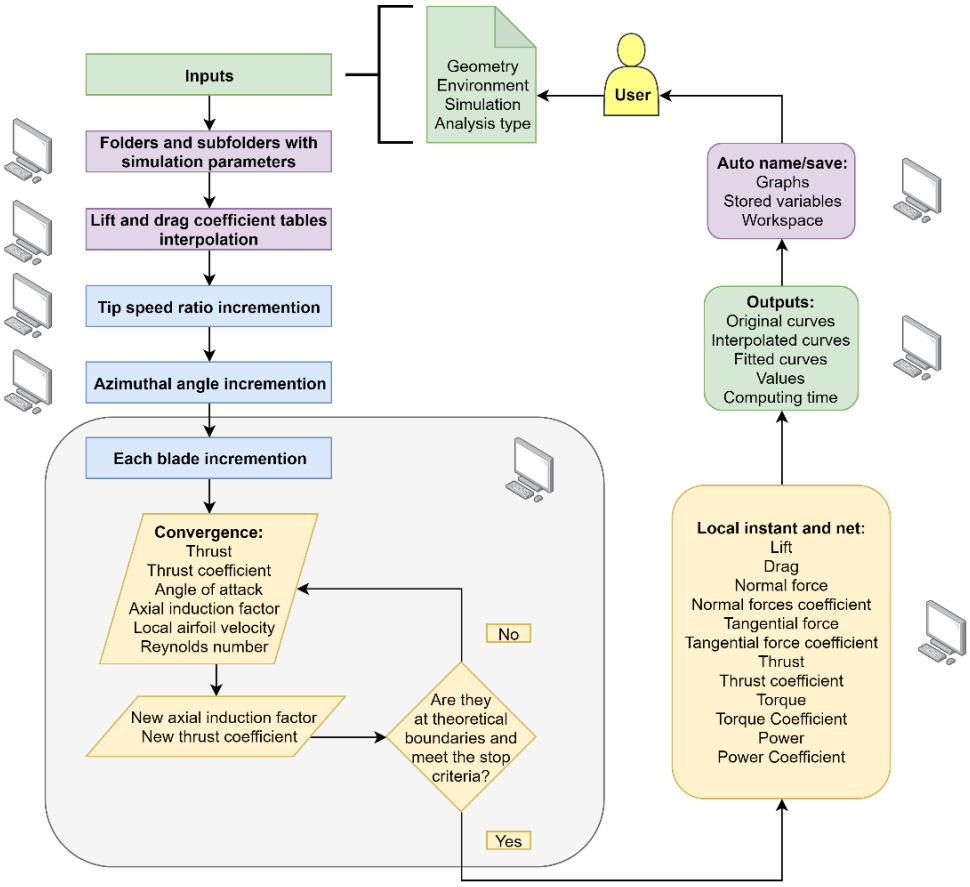

Figure 2. Method code block diagram

Hypotheses were assumed for those calculations:

- Homogeneous free stream velocity, with perpendicular direction to the actuator disk;
- Steady state flow;
- Incompressible flow (constant density);
- Flow velocities are induced in the axial direction only (perpendicular to the actuator disk);
- Infinite number of blades in the actuator disk;
- Self-starting behavior is neglected;
- The flow is not disturbed by core structures, such as the tower.

2.2 Aerodynamic modelling

The TSR (λ) is the ratio between the tangential velocity and the free stream velocity (V_∞), as described in Eq. (1), which can be rearranged to calculate the angular velocity (ω), as in Eq. (2).

$$\lambda = \frac{\omega R}{V_\infty} \tag{1}$$

$$\omega = \frac{\lambda V_\infty}{R} \tag{2}$$

In Eq. (1) and Eq. (2), R is the rotor radius, which is an input variable. Most simulations were conducted with a TSR step value of 0.1, in order to reduce the computing time.

Each blade of the rotor has an identification number. The code sets the initial position of the blades with the first blade (blade one) in the azimuthal angle (θ) of $\pi/180$ rad (1°). The azimuthal angle of first blade is the reference, which was incremented in values of $\pi/180$ rad (1°). The code analyzes the number of blades, in order to calculate the angle between them and the initial position of each one.

The azimuthal angle step may be considered high, leading to a low level of refinement. However, the values of lift coefficients (C_l) and drag coefficients (C_d), changing with the angle of attack (α), which is related to the azimuthal angle, and Reynolds number (R_e), are experimental (Sheldahl and Klimas [4]). They are necessary for a range of 2π rad (360º) and several values of Reynolds number. Since the literature data is still scarce on those requirements, most of the sources present values of lift and drag coefficients in even higher steps of angle of attack. In order to achieve steps of $\pi/180$ rad (1°), the code performs automatic interpolations, because it is programmed to read and increment the azimuthal angle on this value, which leads to a faster analysis (Fig. 3). Furthermore, excessive interpolation of input data makes the code propagate and improve the errors in the entire analysis. Hence, interpolating or fitting the curves of results is preferable. The user may use analysis type inputs to request additional curves, which are polynomial fitting (with its degree as input) and curve smoothing based on moving average filters. Original curves are always plotted.

Table number			
Lift Coefficients	**Drag Coefficients**	**Angles of Attack**	**Reynolds Number**
C_l (α=1°, R_e=$R_{e,t}$)	C_d (α=1°, R_e=$R_{e,t}$)	1°	$R_{e,t}$ (present table)
C_l (α=2°, R_e=$R_{e,t}$)	C_d (α=2°, R_e=$R_{e,t}$)	2°	
C_l (α=3°, R_e=$R_{e,t}$)	C_d (α=3°, R_e=$R_{e,t}$)	3°	
⋮	⋮	⋮	interpolation
C_l (α=180°, R_e=$R_{e,t}$)	C_d (α=180°, R_e=$R_{e,t}$)	180°	
⋮	⋮	⋮	
C_l (α=360°, R_e=$R_{e,t}$)	C_d (α=360°, R_e=$R_{e,t}$)	360°	

Figure 3. Lift and drag coefficients versus angle of attack table layout

In the absence of literature data on the lift and drag coefficients for the entire range of angles of attack, one can use extrapolation methods. While the lift coefficient values may be close to the real case, this may not be the case of the drag coefficient values.

For the azimuthal angle and blade number increments, the axial induction factor (a) starts to converge. The first calculation uses the initial guess, usually set as 0. The analytical values of thrust over the actuator disk (T) and thrust coefficient (C_T) are calculated through Eq. (3) and Eq. (4) (Biadgo *et al.*, [8]).

$$T = 2\rho A a(1-a)V_\infty^2 \tag{3}$$

$$C_T = 4a(1-a) \tag{4}$$

In Eq. (3), A is the the area crossed by the flow, calculated through the rotor height (H) and radius (Eq. (5)), and ρ is the fluid density, which are all inputs for the code.

$$A = 2RH \tag{5}$$

The core velocity, V_c, (Eq. (6)) and the downstream velocity, V_w, (Eq. (7)) are estimated with the analysis current value of the axial induction factor, which starts through the initial guess.

$$V_c = V_\infty(1-a) \tag{6}$$

$$V_w = V_\infty(1-2a) \tag{7}$$

Equation (7) shows a simplifying hypothesis used in the SST model, which is to consider the same behavior of the flow upstream and downstream. However, for the calculation of the local velocity over the airfoil (V_r), different expressions are used for each of those areas, as shown in Eq. (8) and Eq. (9).

$$V_r = \sqrt{\left[\omega R + \left(\frac{V_c + V_\infty}{2}\right)\cos(\theta_i)\right]^2 + \left[\left(\frac{V_c + V_\infty}{2}\right)\sin(\theta_i)\right]^2}\text{, for } 0 \le \theta_i \le \pi \tag{8}$$

$$V_r = \sqrt{\left[\omega R + \left(\frac{V_c + V_w}{2}\right)\cos(\theta_i)\right]^2 + \left[\left(\frac{V_c + V_w}{2}\right)\sin(\theta_i)\right]^2}\text{, for } \pi < \theta_i < 2\pi \tag{9}$$

The azimuthal angle is referred as θ_i because it changes with the blade. The reference azimuthal angle (first blade) is the one inserted in the x-axis of resulting curves. With the local velocity, it is possible to calculate the Reynolds number, as in Eq. (10).

$$R_e = \frac{\rho V_r c}{\mu} \tag{10}$$

In Eq. (10), c is the constant chord of the blade and μ is the fluid dynamic viscosity. A Reynolds number initial average estimation ($R_{e,avg}$) may be used for the whole analysis, however it may lead to highly unrealistic results, depending on the analysis case. The only advantage is a possible computational effort reduction. In order to estimate it, the analysis TSR average ($\bar{\lambda}$) is calculated (Eq. (11)). As in Eq. (2), the angular velocity average ($\bar{\omega}$) is derived (Eq. (12)). For high differences between the initial TSR value ($\lambda_{initial}$) and final TSR value (λ_{final}), the local velocity over the airfoil is assumed as the tangential velocity, which is also an average. This may be a reasonable approximation only if the initial TSR value is much higher than 1, which means that the tangential velocity is much higher than the free stream velocity, neglected in this calculation. Then, Eq. (10) is rewritten as in Eq. (13). In spite of being an option, it is not recommended to proceed the analysis with the Reynolds number estimation, as the computing time reduction may not justify the risk of generating unrealistic results. The main purpose of estimating the Reynolds number through Eq. (11), Eq. (12) and Eq. (13) is to compare its results to others, in order to assess whether particular cases can be analyzed in that way.

$$\bar{\lambda} = \frac{\lambda_{final} - \lambda_{initial}}{2} \tag{11}$$

$$\bar{\omega} = \frac{V_\infty \bar{\lambda}}{R} \tag{12}$$

$$R_{e,avg} = \frac{\rho \bar{\omega} R c}{\mu} \tag{13}$$

Instead of using the chord as an input, the solidity (σ) may be used as well, which depends on the radius, chord and number of blades (N) as defined by Eq. (14).

$$\sigma = \frac{Nc}{2R} \tag{14}$$

In order to select the values of lift and drag coefficients, the local instantaneous angle of attack is calculated through Eq. (15), considering that there are no pitch/twist angles along the blade (Biadgo *et al.* [8]).

$$\alpha = \tan^{-1}\left[\frac{V_c \sin(\theta_i)}{V_c \cos(\theta_i) + \omega R}\right] \tag{15}$$

With the values of Reynolds number and angle of attack, the code starts an analysis over the lift and drag coefficient tables. They are organized in Excel sheets, each corresponding to a Reynolds number. The coefficients are listed as a function of the angle of attack. For each calculation, the Reynolds number is analyzed, and the sheet corresponding to the closest value is selected (this is done once, in case of using the initial Reynolds number average estimation, with no interpolations related to this value). These values are used to compute the local instantaneous normal force coefficient (C_n) and tangential force coefficient (C_t), as described through Eq. (16) and Eq. (17), respectively. From these coefficients, the local instantaneous thrust (T_i) is derived (Eq. (18), Biadgo *et al.* [8]).

$$C_n = C_l \cos(\alpha) + C_d \sin(\alpha) \tag{16}$$

$$C_t = C_l \sin(\alpha) - C_d \cos(\alpha) \tag{17}$$

$$T_i = 0.5\rho V_r^2 Hc[C_n \sin(\alpha) - C_t \cos(\alpha)] \tag{18}$$

Equation (18) describes the method to calculate the local instantaneous thrust with experimental lift and drag coefficient values. The thrust calculated from Eq. (3) represents the summation of all blades in an instant, while the thrust calculated from Eq. (18) represents the instantaneous contribution of a single blade. However, the coefficients can be compared in order to converge the axial induction factor value. Hence, the net and local instantaneous thrust are assumed the same at this part of the analysis. It is important to observe that this may lead to under prediction of the wake effects of one blade on the others. However, the equations described in this work are derived from methods in which the wake can be considered, through simplifying hypotheses. As a result, the prediction on rotors of low number of blades is expected to be more precise.

The instantaneous local thrust coefficient (C_{Ti}) is calculated using the result of Eq. (18) through Eq. (19).

$$C_{Ti} = \frac{T_i}{0.5\rho V_\infty^2 A} \tag{19}$$

To converge the axial induction factor, the results of Eq. (19) and Eq. (4) are compared, leading to a new value, calculated rearranging Eq. (4), which leads to Eq. (20).

$$a = 0.5\ \ 1 - \sqrt{1 - C_T} \tag{20}$$

The local instantaneous torque in a blade (Q_i) is generated by local instantaneous tangential force (F_t), while the local instant thrust of Eq. (18) is also related to the local instantaneous normal force (F_n). Those forces depends on the local instantaneous lift (L) and drag (D), forces (Eq. (21) and Eq. (22), respectively).

$$L = 0.5\rho Hc V_r^2 C_l \tag{21}$$

$$D = 0.5\rho Hc V_r^2 C_d \tag{22}$$

Using the results of Eq. (21) and Eq. (22), instantaneous local tangential and normal forces can be

calculated (Eq. (23) and Eq. (24), respectively).

$$F_t = L\sin(\alpha) - D\cos(\alpha) \tag{23}$$

$$F_n = L\cos(\alpha) + D\sin(\alpha) \tag{24}$$

The instantaneous local torque is described by Eq. (25).

$$Q_i = F_t R \tag{25}$$

Since the code considers a single-bladed turbine at each iteration, as described before, a local instantaneous torque coefficient (C_{Qi}) can be derived, leading to Eq. (26). The net torque (Q) is obtained adding the local instantaneous values for all blades, and its average in one revolution ($\bar{Q}$) leads to the torque coefficient (C_Q) described in Eq. (27).

$$C_{Qi} = \frac{Q_i}{0.5\rho V_\infty^2 RA} \tag{26}$$

$$C_Q = \frac{\overline{Q}}{0.5\rho V_\infty^2 RA} \tag{27}$$

The local instantaneous power (P_i) extracted from the wind in a single blade also can be derived, leading to Eq. (28).

$$P_i = \omega Q_i \tag{28}$$

Adding the values of the instantaneous local power of all blades leads to the net instantaneous wind extracted power (P). An analytical relation between the extracted power and the axial induction factor is given through Eq. (29), as described by Biadgo *et al.* [8].

$$P = 0.5\rho A a(1-a)^2 V_\infty^3 \tag{29}$$

From the power associated with the flow (P_{flow}), described in Eq. (30), the power coefficient (C_P) can be calculated, as in Eq. (31).

$$P_{flow} = 0.5\rho V_\infty^3 A \tag{30}$$

$$C_P = \frac{P}{P_{flow}} \tag{31}$$

As commented before, in this work the power coefficient is treated as the aerodynamic efficiency, while most authors consider it as the overall efficiency. The present authors had to use the power coefficient equivalence to the overall machine efficiency in order to be able to compare with the present predictions with the available experimental results.

Figure 4 shows the geometry and the variables involved. Further details on the computational description of the method are included together with the validation, in order to justify the choice of the parameters.

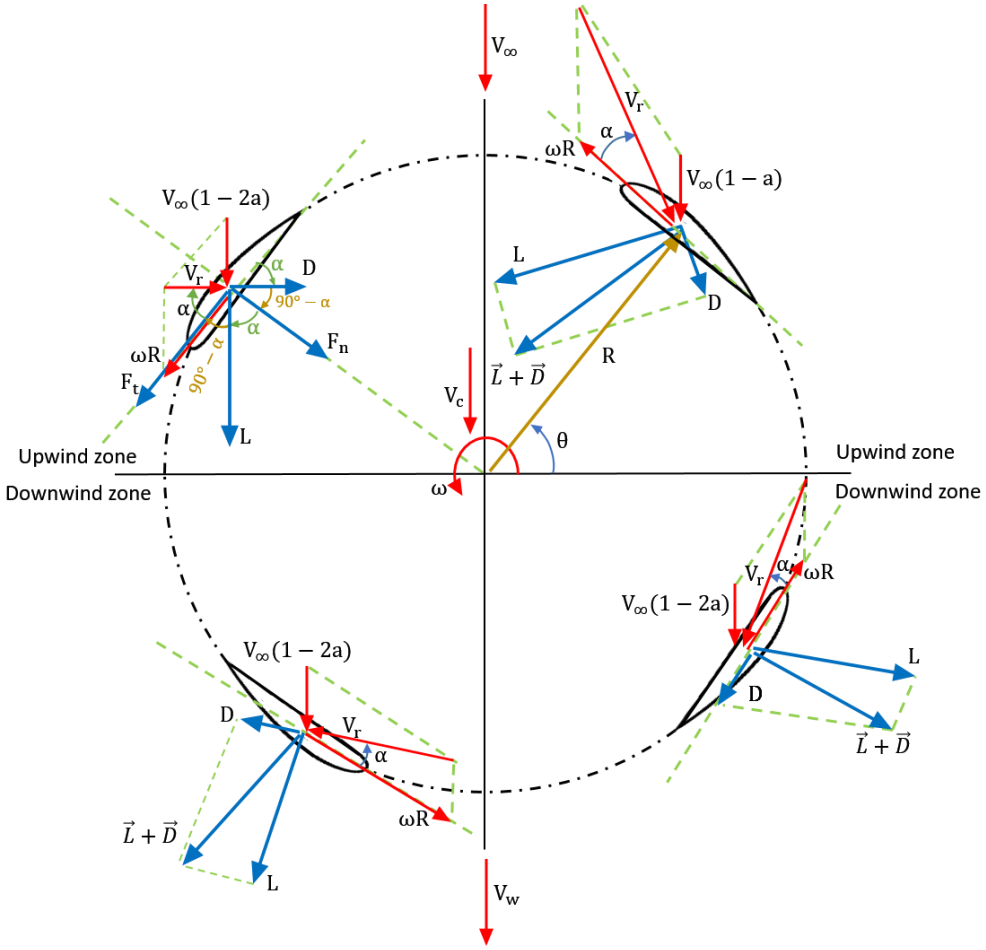

Figure 4. Geometry and variables of H-VAWT

3 Numerical treatment

3.1 Optimization of the calculation parameters

As the level of refinement of the simulations is increased, better results are expected, until a limit in which the successive results present negligible changes. However, the refinement increases the computing time significantly. The optimization study is important to define this limit, ensuring the achievement of good results with the lowest refinement level. In order to evaluate the optimum parameters for the simulation, the H-VAWT described in the literature through other method of analysis and experimental results was simulated using the present method. Geometry and environmental parameters were set as close as possible to the literature description, defining the basis for the optimization investigation. Grid values such as the time and azimuthal angle increments are fixed, due to the use of experimental results of lift and drag coefficients.

Since one of the objectives of the present paper is also to achieve a low computational effort method, the computing time and the specifications of the computer used in the simulations are important parameters.

Specifications of the computer

A home computer was used to perform the simulations, composed by an Intel Core i7 7700 processor (4 cores, 8 Mb cache, 3.6 GHz base clock and 4.2 GHz in Turbo Boost mode), 16 GB DDR 4 RAM, with 2133 MHz frequency and a Radeon RX 550 2 GB GDDR5 GPU.

Basic simulation parameters

The basic input values (or basic simulation parameters) are built based on Castelli *et al.* [9] (Table 1).

Table 1. Input values described by Castelli *et al.* [9]

Input	Value
Free stream velocity (m/s)	9
Air density (kg/m³)	1.225
Rotor radius (m)	0.515
Rotor swept area (m²)	1.236
Rotor solidity	0.5
Rotor height (m)	1.4564
Number of blades	3
Blades airfoil	NACA 0021
Blades chord (m)	0.0858

Among the values of swept area and radius, only one needs to be provided, since the other is calculated through the height. Considering the actuator disk method used in this work, the swept area is the projected crossing area, defined as the product of the rotor diameter ($2R$) and height (H), which results in a different value (1.5 m²). However, by substituting Eq. (29) and Eq. (30) in Eq. (31), it is possible to observe the low influence of the swept area on the power coefficient, which is an additional reason for the use of this parameter in the optimization test.

As occurs to the swept area and radius, Eq. (14) shows the need of selecting either the chord length or the solidity as an input. Since Castelli *et al*. [9] have used a different definition for the solidity, the chord was chosen as the basic input.

The values of fluid dynamic viscosity and overall machine efficiency were assumed. They are described with other design and simulation parameters in Table 2. The values in Table 1, Table 2 and Table 3 describe the base rotor and simulation parameters used as starting conditions for the optimization.

Table 2. Simulation, design and assumed values used in the base input set

Input	Value
Air dynamic viscosity (Pa.s)	0.0000183
Overall machine efficiency	0.9
TSR initial value	1
TSR final value	3.5
TSR step size	0.1
Axial induction factor initial guess	0
Axial induction factor convergence criteria	$a_{i+1} - a_i \leq 0.001$
Maximum number of convergence iterations	10,000
Degree of polynomial fitting	6
Analysis type inputs	-

The axial induction factor convergence criteria refers to the difference between a new axial induction factor (a_{i+1}) obtained and its previous value (a_i). The simulation can be refined decreasing this value, however it might lead to a higher level of computational effort, unless the convergence is reached at the first iterations. Since it is unknown if all axial induction factor calculations converge and, if so, the maximum number of convergence iterations needed in an analysis, it is necessary to define a limit, avoiding an infinite loop process. In order to maximize the number of converged iterations, a value of 10,000 was set as the maximum.

Table 3. Analysis type inputs used in the base input set

Analysis type inputs	Value
Joukowski (1) / regular airfoil (0)	0
Use swept area (1) / radius (0)	0
Use chord length (1) / solidity (0)	1
Local instant Reynolds number (1) / estimation (0)	1
Interpolate lift and drag coefficients with Reynold number (1) / use closest table values (0)	1
Apply machine efficiency on power coefficient (1) / do not apply (0)	1
Generate smoothed curves (1) / do not generate (0)	0
Variable number of blades analysis (1) / only constant (0)	0

The interpolation of lift and drag coefficient tables with the angles of attack is always performed, using more processing time than interpolating different tables with the Reynolds number. The Reynolds number interpolation also tends to generates better results.

It is important to observe the computing time dedicated to the calculations and to the graphs generation separately, since in a fast analysis, graph generation takes a considerable percentage of the whole analysis. For this reason, the base simulation did not include the generation of smoothened curves.

The first optimization parameter to be changed is the TSR step size, with all the other parameters maintained the same. Four simulations were performed for different decreasing values of TSR step, as described in Table 4. Simulation number 3 is based on the base input parameters. The analysis of the average power was chosen due to the noticeable difference of its values for the different simulations. The percentage difference of average power and computing time between each simulation are computed as well, in order to help the choice of the optimum case.

Table 4. TSR step size change – simulations 1 to 4

Simulation Number	1	2	3	4
Average Power (W)	101.78	102.13	104.74	105.25
Absolute Difference (%)	0.00	0.34	2.56	0.49
Analysis Time (s)	34.01	35.22	51.65	173.41
Absolute Difference (%)	0.00	3.56	46.65	235.74
TSR Step	0.3	0.2	0.1	0.01

The highest absolute difference in average power was observed between TSR step sizes of 0.2 and 0.1 (2.56%), corresponding to simulations 2 and 3. Between TSR step sizes of simulations 3 (0.1) and 4 (0.01), the average power difference decreased to 0.49%, with a significant increase of the simulation time (235.74%). Furthermore, the value of 0.1 is sufficient for generating discrete curves. Therefore, the TSR step size of 0.1 (which was set as a base simulation parameter) presented the best balance between the accuracy of the results and the computing time.

The next optimization parameter analyzed is the axial induction factor convergence criteria, investigated in the simulations 5 to 7. For this case, simulation 6 is the same as 3, with the base input parameters set (Table 5).

Table 5. Axial induction factor convergence criteria change – simulations 5 to 7

Simulation Number	5	6	7
Average Power (W)	104.72	104.74	104.74
Absolute Difference (%)	0.00	0.02	0.00
Analysis Time (s)	31.26	51.65	82.72
Absolute Difference (%)	0.00	65.23	65.15
Induction Factor Convergence Criteria	0.01	0.001	0.0001

From axial induction factors convergence criteria of 0.01 and 0.001, there is a small difference of 0.02% on the average power. The difference on the average power is 0 from a convergence criteria of

0.001 to 0.0001, however the computing time is 65.15% higher.

Finally, the last main optimization parameter analyzed is the maximum number of iterations for axial induction factor convergence. In this case, simulations 8 to 12 were defined. Simulation 12 is based on the base parameters.

Table 6. Induction factor maximum number of convergence iterations – simulations 8 to 12

Simulation Number	8	9	10	11	12
Average Power (W)	104.74	104.74	104.74	104.74	104.74
Absolute Difference (%)	0.00	0.00	0.00	0.00	0.00
Analysis Time (s)	32.87	34.00	37.60	40.06	51.65
Absolute Difference (%)	0.00	3.44	10.59	6.54	28.93
Maximum Convergence Iterations	100	500	2000	5000	10000

Simulations 8 to 12 show the same average power, with an increase of the computing time for higher values of maximum number of convergence iterations. A possible explanation is the predominance of low number of convergence iterations on needed values of axial induction factors. Hence, the additional computing time may be related to the values that did not converge. From this, it is possible to conclude that either the induction factors converged in few iterations, or they did not converge, for all or most processes in this analysis case.

For this case, simulations 8 to 12 produced the same results, and the lowest running time was achieved through simulation 8. It is prudent to assume the parameters of simulation 9 as the best reference, due to the fact that other analysis cases may require more than 100 convergence iterations to successfully reach the convergence criteria. Furthermore, a difference of 3.44% in time, may be considered low enough.

3.2 Validation

Using the base inputs described before, as well as the best optimization case, two simulation were performed by the present method in order to evaluate the wind turbine behavior.

The resulting power coefficient curves versus TSR (original, without polynomial fitting or curve smoothing) were plotted together with the experimental and CFD results presented by Castelli *et al*. [9] and the Betz limit, as a reference for the maximum theoretical power coefficient (Fig. 5).

The total analysis time for the base simulation parameters was 51.65 seconds, in which approximately 24.53 seconds were used for generating more than 40 different graphs. The optimized parameters led to a running time of 34 seconds.

The predicted power coefficient results were very close to the experimental results at the lowest and highest values of TSR. For a TSR of 3.3, the present result of power coefficient (0.255) is only 2% higher than the experimental value (0.25). Between TSR values of approximately 2.2 and 2.8, a fast divergence of both curves is observed. In addition, the limited number of tables of lift and drag coefficients against the angle of attack, may not have generated realistic coefficients of TSR values. After that, the curves rapidly approached to each other again. For TSR values lower than 2.2 and higher than 3, it is possible to observe good agreement between the results.

It is important to remember that there is a difference between the solidity definitions presented in the present work (Eq. (14)) and in Castelli *et al*. work ($\sigma = Nc/R$) [9]. For this reason, another simulation was performed, considering the solidity of 0.5 instead of the chord, which led to a different curve. In this case, the optimum parameters were used, and the resulting curve presented higher differences from experimental results for the lowest and highest TSR values analyzed, however the difference for TSR values between them became smaller. This results is presented in Fig. 5.

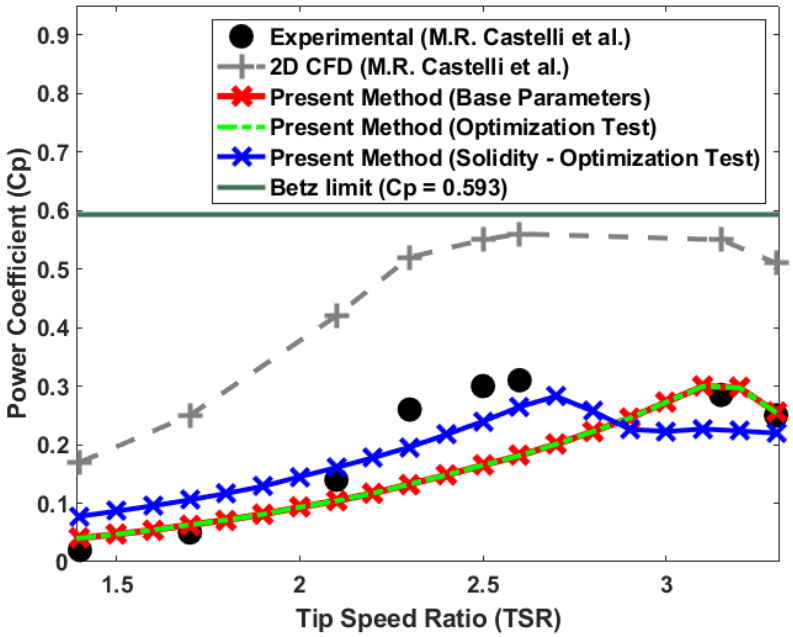

Figure 5. Power coefficient versus TSR curves of validation: Castelli *et al*. [9] (experimental and 2D CFD) and the present method

The CFD results presented by Castelli *et al*. [9] follow the same tendencies as the experimental results, with a clear over prediction of the power coefficient. The present predictions seem to agree better with the experimental results than the numerical calculations of Castelli *et al*. [9].

Castelli *et al*. [9] reported a total CPU time of about 4 days for each simulation, on an 8 processor with 2.33 GHz clock frequency computer. Compared to the 34 seconds of the present optimized simulation, it is possible to conclude that the low computational effort is successfully achieved.

4 Results and discussion

In addition to the previous results and discussion, further simulations were performed, based on other changes in the simulation base parameters (Table 7).

Table 7. Parameters change from validation base input set – simulations 13 to 16

Simulation Number	Changed parameters
13	No lift and drag coefficients interpolation with Reynolds number
14	Reynolds number estimation for whole analysis
15	Generation of smoothed curves
16	TSR step, induction factor convergence criteria, generation of smoothed curves

Values of power and power coefficient for a TSR of 2.2 were selected as it is close to the average TSR value. Besides the average power values, the maximum power values were also included. As expected, simulations 13 and 14 generated similar results. The Reynolds number is important for selecting the best lift and drag coefficients data available. Therefore, even with a poor estimation, the table selected in simulation 14 may contain similar data compared to the tables used in simulation 13. The higher analysis time in simulation 13, compared to simulation 14, is an evidence of the considerable computational effort taken for searching and scanning tables. Since simulation 15 is the same as the base input values (represented by simulations 3, 6 and 12 as well), with the difference of the generation of smoothed graphs, the results did not change. However, the analysis time was 74.95% higher, reflecting

the high number of additional graphs generated. The similar results of simulations 13 and 14 are very different from the results of simulation 15, as shown in Table 8 and in Fig. 6.

Table 8. Results and computing times for simulations 13 to 16

Simulation Number	13	14	15	16
Power Coefficient (TSR=2.2)	0.2822	0.2822	0.1169	0.117
Absolute Difference (%)	0.00	0.00	1.41	0.00
Power (TSR=2.2) (W)	189.10	189.10	78.33	78.34
Absolute Difference (%)	0.00	0.00	141.41	0.01
Maximum Power (W)	232.10	232.11	223.12	238.90
Absolute Difference (%)	0.00	0.00	3.87	7.07
Average Power (W)	145.23	145.24	104.74	105.25
Absolute Difference (%)	0.00	0.01	38.67	0.49
Analysis Time (s)	209.36	65.36	90.86	820.71
Absolute Difference (%)	0.00	220.32	39.01	823.27

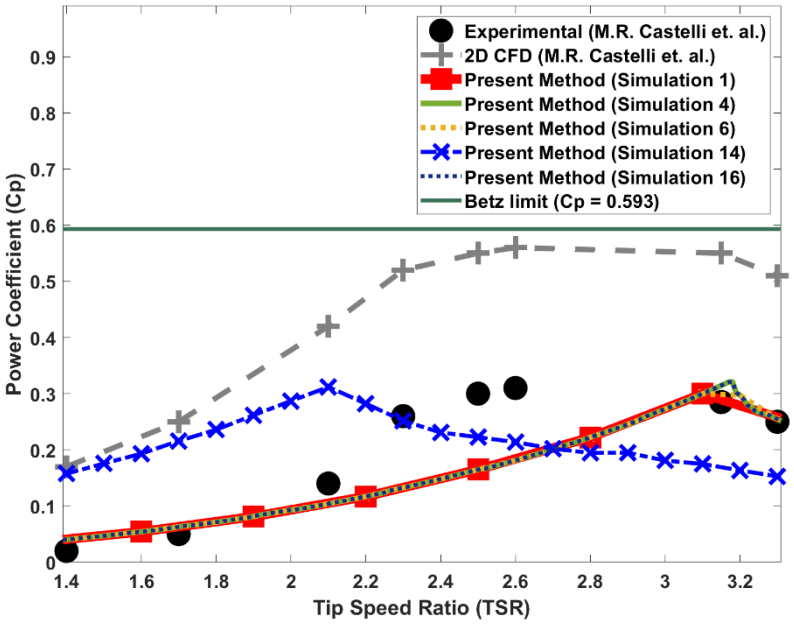

Figure 6. Power coefficient versus TSR curves: Castelli *et al*. [9] (experimental) and present method (simulations 1, 4, 6, 9 and 14)

Even with a high refinement level, simulation 16 presented a small difference in the resulting average power, compared to simulation 15 (0.49%). However, the computing time raised to 823.27%, which represents a big difference.

Other important results are the thrust and torque with time or azimuthal angle, calculated for each blade and the sum of all blades. The fluctuations of those curves represent important parameters for the turbine balance estimation. Some of those curves for the base input values are shown in Fig. 7 and Fig. 8, as they are generated at the end of the analysis.

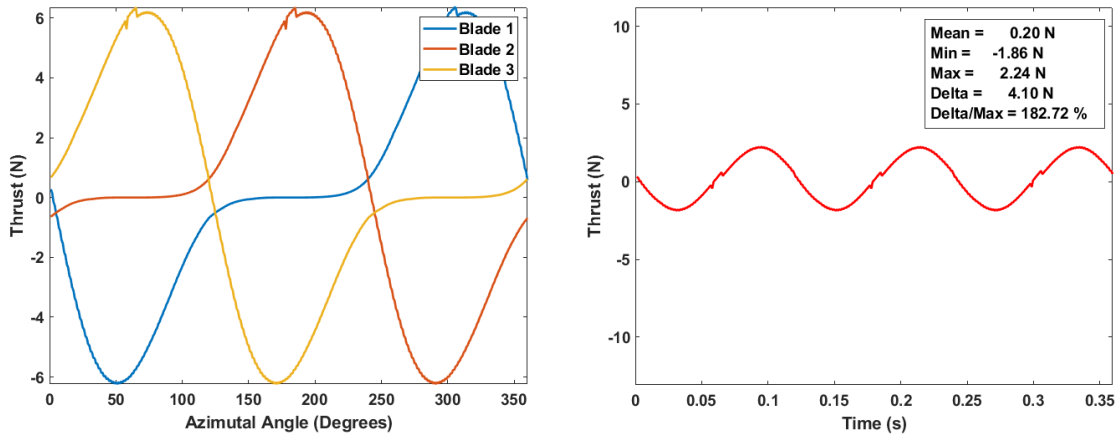

(a) (b)

Figure 7. Thrust curves: (a) with time azimuthal angle for each blade; (b) sum of all blades with time

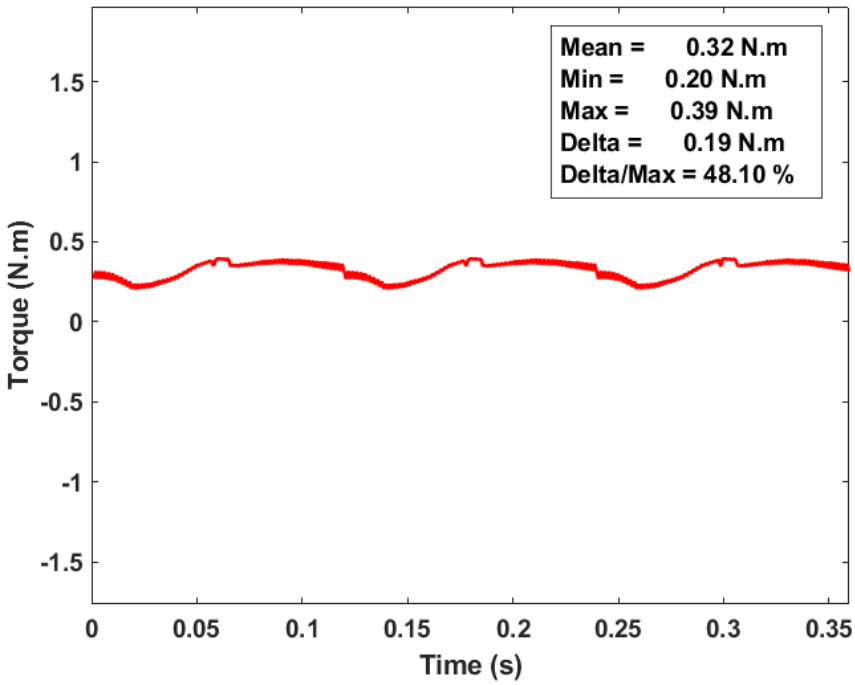

Figure 8. Sum of all blades torque with time (validation case)

The minimum (Min), maximum (Max) and difference between them (Delta) over the maximum values (Delta/Max) of thrust, as well as for the torque, indicated on Fig. 7b and Fig. 8, are used to estimate the mechanical stresses and balance over the turbine structure. The balance of 182.72% on the thrust (Fig. 7b) is considered poor. However, this effect may be minimized by the lower corresponding value of 48.10% for the torque (Fig. 8). Considering the small dimensions of the validation VAWT, those values became even harder to predict.

Poor balance values tends to produce higher impacts on large-size VAWTs, which is not the case of the validation rotor. This may be verified through the values of mean, minimum and maximum thrust and torque, which are low.

5 Conclusions

In this work, a simple computational method for predicting the behavior of straight-bladed vertical axis wind turbines is described. The method is derived from other consolidated methods, with some changes. After the selection of base input values, optimization and validations tests have been used in order to verify the effectiveness of the method. For a good part of the tip speed ration domain, the results of the power coefficient have been considered satisfactory. For a small range of TSR, the disagreement between experimental and calculated results increased. Even for these cases, the predictions may be considered better than other sophisticated methods.

The other main objective of achieving a low computational effort code, has been successfully reached, a small computing time of 34 seconds for optimized simulation. Another noticeable finding is the tendency of fast convergence.

Acknowledgements

The first author wishes to thank the Instituto de Pesquisas Eldorado (Eldorado Research Institute) for the financial support.

The second author wishes to thank the *Conselho Nacional de Desenvolvimento Científico e Tecnológico* (*CNPq*) for the PQ Research Grant **304372/2016-1**.

The authors thank the Faculty of Mechanical Engineering (FEM) and the State University of Campinas (Unicamp) for providing the necessary additional structure used during the period of this work.

References

[1] E. Möllerströma, P. Gipe, J. Beurskens and F. Ottermo. A historical review of vertical axis wind turbines rated 100 kW and above. *Renewable and Sustainable Energy Reviews 105*, pp. 1–13, 2019.

[2] D. Gang and W. C. Kau. Unsteady Flow Numerical Simulation of Vertical Axis Wind Turbine. *Procedia Engineering*, vol. 99, pp. 734-740, 2015.

[3] A. Rezaeiha, H. Montazeri and B. Blocken. Towards accurate CFD simulations of vertical axis wind turbines at different tip speed ratios and solidities: Guidelines for azimuthal increment, domain size and convergence. *Energy Conversion and Management*, n. 156, pp. 301–316, 2018.

[4] R. E. Sheldahl and P. C. Klimas. Aerodynamic Characteristics of Seven Symmetrical Airfoil Sections Through 180-Degree Angle of Attack for Use in Aerodynamic Analysis of Vertical Axis Wind Turbines, Sandia National Laboratories and Livermore for The U.S. Department of Energy, March 1981.

[5] R. F. Mikkelsen. Actuator Disc Methods Applied to Wind Turbines. Kgs. Lyngby, Denmark: Technical University of Denmark (DTU). MEK-FM-PHD, n. 2003-02, 2004.

[6] R. E. Froude. On the Part Played in Propulsion by Difference in Pressure. *Transactions of the Institution of Naval Architects*, p. 390-423, 1889.

[7] R. J. Templin. Aerodynamic performance theory for the NRC vertical-axis wind turbine. NRC Lab. report LTR-LA-190, p. 29, June, 1974.

[8] A. M. Biadgo, A. Simonovic, D. Komarov and S. Stupar. Numerical and Analytical Investigation of Vertical Axis Wind Turbine. FME Transactions n. 41, pp. 49-58, 2013.

[9] M. R. Castelli, A. Englaro and E. Benini. The Darrieus wind turbine: Proposal for a new performance prediction model based on CFD. Energy n. 36, pp. 4919-4934, 2011.